Reference: Abstract published in the 16th Annual Lunar and Planetary Institute Summer Intern Conference Proceedings, pp. 28–30, July, 2000. The proceeding is available through the LPI, and the abstract is available through www.lpi.usra.edu/science/kirkland

Surface Composition of Mars: Examination of Syrtis Major Using Thermal Infrared Data. Jennifer Ward, Colgate University, Hamilton, NY; *Advisor:* Laurel Kirkland, Lunar and Planetary Institute, Houston, TX

Introduction. An important goal of Martian infrared studies is to determine surface mineralogy, enabling scientists to locate deposits of interesting minerals (e.g. carbonates, sulfates) for landing site selection. Currently, the Global Surveyor Thermal Emission Spectrometer (TES, 6–50 μm) is returning infrared data from Mars that can be used to search for such minerals.

Syrtis Major is one of the prominent low-albedo regions of Mars, and is believed to be a low relief shield volcano [e.g. 1]. However, it has an unexpectedly moderate thermal inertia, implying the presence of coarse-grained material [2,3]. It was chosen because of its reasonably low relief and the likelihood of a relatively strong spectral signature commonly associated with low-albedo TES data ([4] and our findings).

Christensen et al. [4] have found calcium-rich pyroxene to be the best match to TES spectra of the low-albedo region, Cimmeria. Mustard et al. [5,6] assert that both low and high calcium pyroxenes compose the dark region of Syrtis Major. Bandfield et al. [7] cite two likely compositions for the low-albedo regions of Mars: (1) a clinopyroxene and plagioclase feldspar dominated basalt and (2) a volcanic glass and plagioclase feldspar dominated andesite. They propose that NW Syrtis Major has an andesitic composition, while the majority of Syrtis is in the basaltic regime [7]. Many believe that the dark regions are composed of more coarse particles than the bright regions [e.g. 8,9], with Syrtis in particular containing sand-sized particles [3]. The purpose of this project is to test the assertions described above.

Background. Rocks emit as blackbodies, except where there are molecular absorptions or scattering effects. Absorptions occur at characteristic wavelengths due to variations in the chemistry and configuration of the elements present. These factors dictate the regions that do not exhibit blackbody behavior. The signal received will thus be weakened and show absorption bands in characteristic regions. Even minerals composed of similar elements are distinctive due to the various bending and stretching vibrations of their constituents. Silicates, for example, have intense absorption bands that occur between 8 and 12 μm, which are the result of asymmetric Si–O–Si stretching vibrations [10]. Figure 1 shows a typical Mars signature plotted with a Planck curve, which exhibits characteristic atmospheric and surface absorptions.

Before infrared radiation is detected by TES, it passes through a layer of atmospheric dust and gases. The radiance measured will have absorption features caused by the atmosphere as well as the mineral(s) that characterize the source region. Thus the spectra contain features of this aerosol, which must be removed in order to view the true surface spectra. With some reasonable simplifications [11], the measured radiance (L_{obs}) can therefore be defined as:

$$L_{obs} = \tau \cdot L_s + L_{up} \quad (1)$$

where τ is the atmospheric transmission, L_s is the radiance of the source, and L_{up} is the re-emission of the dust, which exists because the aerosol has a temperature [11]. Solving the above equation for L_s gives information about the surface.

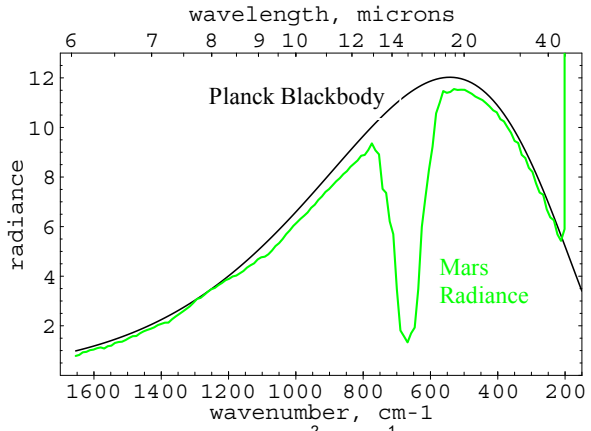

Figure 1: Radiance is in watts/m^2 ·sr·cm^{-1}.

Figure 2 shows the calculated atmospheric transmission spectrum. The uncorrected TES spectra most resemble this spectrum, which shows that a strong aerosol signature must be removed to see the surface spectrum. The result is a spectrum of emitted radiation from the surface, which is extremely subtle when compared to the transmission spectrum (Figure 2). For a more detailed explanation of atmospheric removal techniques, see [11].

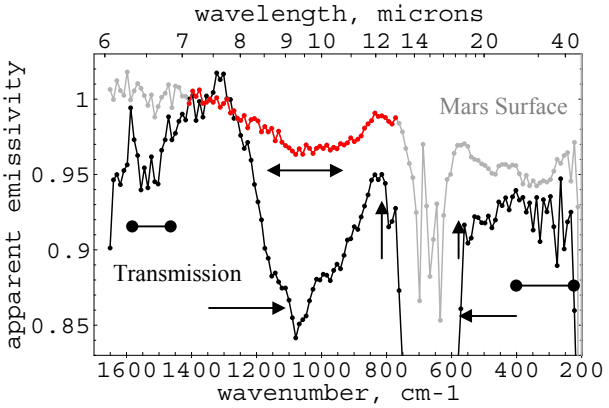

Figure 2: The Mars surface spectrum shows the full spectral range measured by TES. The dark shading in the Mars surface curve corresponds to the region looked at in this study. Arrows point to CO_2 absorption features, and double circles indicate water vapor. Double arrows show the aerosol band.

Procedure. The region of Syrtis sampled was located between –10 - 30° latitude and 285–320° longitude. This incorporates both the western extent of Syrtis and the eastern portion of Arabia, providing for data comparison.

The data used were acquired by TES, which is a Michaelson Interferometer with an unapodized spectral resolution of 10 or 20 cm^{-1}. Most of the data were taken at 20 cm^{-1}, used in this study. The spatial resolution of the instrument is ~3 km [12], with a peak-to-peak signal-to-noise ratio (SNR) of 66 at 10 μm and a 270K blackbody.

TES produced 143 points of radiance data in the wavelength range from 1600 to 200 cm^{-1}, which is in the thermal infrared [13]. We used data from cdroms 134–139, which contain mapping phase data for TES orbits 3888 through 4207. After examining all wavelengths, we limited the wavelength range used from ~1400 to 750 cm^{-1}, using 61 points. We dropped 750–550 cm^{-1} because strong CO_2 gas absorptions inhibit viewing of the surface at these wavelengths. The 1971 IRIS mid-day spectra typically show a 20 µm band accompanying the 10 µm band, which was not observed in the TES data. We removed wavenumbers <550 due to this possible calibration problem. Further, we limited data used to a peak-to-peak signal-to-noise ratio (SNR) above 20 (~100 r.m.s. SNR) at 270 K, which excluded wavenumbers >1400. The peak-to-peak SNR of the TES data was calculated using the method described in [14].

Under Department of Defense-sponsored programs, the Aerospace Corporation developed an In Scene Atmospheric Compensation (ISAC) technique to calculate the atmospheric transmission and re-emission (Equation 1), and we used this technique on the TES data [15].

Observations. Figure 3 shows two TES spectra from NE Syrtis with the atmospheric compensation applied. The top spectrum is from a region with an average TES albedo (0.3–2.7µm) of 0.09 (incidence angle (ina)=44°, emission angle (ema)=0.2°), and the bottom spectrum is from a 0.10 albedo region (ina=45°, ema=0.2°). A better SNR is achieved by averaging several spectra. The overall bowl-shape of these spectra is common in Syrtis's dark regions, with emissivity peaks occurring near 1300 cm^{-1}, followed by a flat shape at higher wavenumber (shorter wavelength).

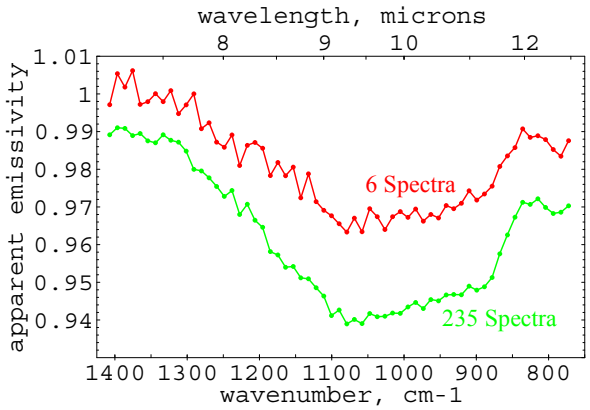

Figure 3: The top curve shows the average of 6 Martian spectra taken from TES orbit 3962. The bottom, gray curve shows the average of 235 spectra taken from orbits 3888 to 4207 in a region approximately 470 by 170 km in size and centered at 12°N latitude, 289° longitude. Note the better signal-to-noise of the bottom curve, which is vertically offset by 0.02 for clarity. This and the following plots show only a subset of the TES data (see Figure 2).

Figure 4 shows another typical dark region spectrum (average albedo=0.10, ina=45°, ema=0.2°) from central Syrtis Major plotted with a bright region spectrum (average albedo=0.27, ina=46°, ema=0.2°). Bright regions are observed to be relatively flat in the 9-µm region, while there is a large dip in emissivity at higher wavenumbers and an emissivity trough near 850 cm^{-1}.

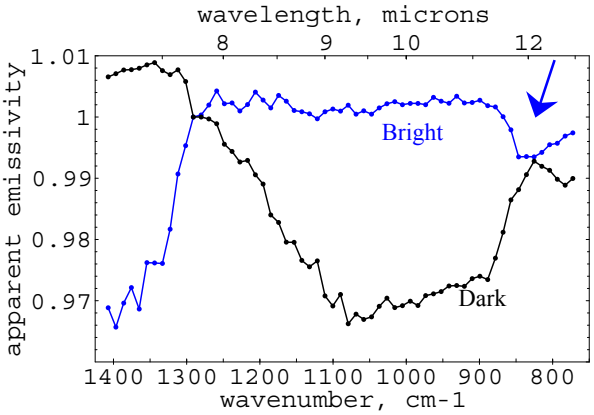

Figure 4: The light gray plot is an average of 746 spectra from orbits 3888 to 4207 in a typical bright region approximately 415 by 850 km in size and centered at 14°N latitude, 313° longitude. The arrow indicates the transparency feature. The dark gray plot is 528 averaged spectra taken from orbits 3888 to 4207 in a dark region roughly 1190 by 290 km in size and centered at 10°N latitude, 293° longitude.

Figure 5 shows the same dark region spectrum as in Figure 4, plotted with data described in [7]. There is not enough information in the spectrum of the dark region examined to make substantive conclusions about the mineralogy. It can be said, however, that the broad U-shaped 9 µm band is consistent with the basalt "Surface Type 1" spectrum described in [7] (Figure 5 bottom curve). It is also broadly consistent with "Surface Type 2", but the flatter band center would indicate less contribution from glassy material. The region plotted in this figure is in central Syrtis Major, which [7] designate as "Surface Type 1."

We compared our surface spectrum to laboratory spectra of andesite and basalt from [10,16], and the overall broad envelope is consistent with that of basalt or andesite. Figure 6 shows the surface spectrum plotted with basalt.

Discussion. We identified three sources of error and uncertainty. (1) SNR: This is straightforward to characterize, and we address it by excluding low SNR data. (2) Systematic radiance errors associated with the instrument calibration [17]: We partly address it by excluding data at wavenumbers <550. (3) Atmospheric compensation: There is no clear method to calculate the uncertainties because we have no independent knowledge of the true atmospheric spectral shape or variation with time. However, sources of uncertainty include (1) the assumption that the atmospheric profile is invariant with latitude and longitude and (2) the assumption that the calculation is fairly insensitive to topography. This was handled by choosing fairly level regions and excluding corrected spectra that exhibit residual atmospheric CO_2 bands.

It can be concluded that the signature obtained for the dark region of Syrtis is consistent with the TES team signature interpreted as basaltic [7]. The presence of a clear band indicates that this region is composed of well crystalline material with a particle size at least comparable to the wavelength [10], which means that rocks could exist. A flattened emissivity is also observed at wavenumbers >1300,

which is also consistent with larger particle sizes. An exact determination of particle size would require knowledge of the percentage of dust coverage and the vesicularity of the materials at the surface. These are unknowns.

The bright region spectrum from Arabia in Figure 4 shows an apparent emissivity near 1 from ~1260 to 900 cm^{-1}. Three observations can be made about this bright region spectrum: (1) there is a feature at ~850 cm^{-1} with a depth of ~0.008 in apparent emissivity (Figure 4), which we interpret as a transparency feature [18]; (2) emissivity decreases sharply toward wavelengths >1260 cm^{-1} (<7.9 μm); and (3) the region is brighter. All of these observations are consistent with finely particulate material [10, 18].

The TES team used two spectral ranges in their study described in [4,7]: ~1300–800 cm^{-1}, and ~500–200 cm^{-1}, and we used 1400–750 cm^{-1} for our study. Over the region of overlap, the spectral shapes agree broadly with results from [4, 7] for dark regions. However, the TES team obtained a blackbody spectrum for bright regions [19], which is contrary to our results.

To best understand the results of this study and to accurately determine the composition of Syrtis Major, a landing site in this region would be highly advantageous [20]. Edget et al. [20] note that it would be favorable to study a region with exposed rocks or large particles, and from our results it seems clear that there are large particles and possibly rocks exposed at the surface of Syrtis. There is no indication of carbonates or sulfates in our study, but if these materials are rough or fine-grained, they would be below the detection limit. This depends on grain size and surface roughness, and therefore "absence of evidence is not necessarily evidence of absence." Again, a sample of dustless rocks in this region would be highly beneficial [20].

One of the most important factors to note as a result of this study is that the atmospheric correction is severely critical: the answer is driven by this correction (note Figure 2). For example, we applied the correction to the Lunae Planum region of Mars, but because the surface signature was so subtle this region had to be abandoned. For Syrtis Major, Figure 5 shows that we have obtained a weaker band than that obtained by the TES team (~ 3% compared to ~5% for these spectra). There are three possible explanations for this discrepancy: (1) the TES team spectra still have residual atmospheric dust, (2) there is some scaling difference between the two data sets, and (3) one of the atmospheric correction techniques needs improvement. It should be realized that the strongest type region signature we found only had a 3% band depth. The importance of the atmospheric compensation is evident.

The main difficulty in making adequate corrections involves the SNR. Also, a higher spectral resolution would increase confidence in the result, but the spatial resolution was not an issue at this level, i.e. in examining the basaltic plains.

In the future, an unambiguous answer for landing site selection is desired. This leads to the need for an intense examination of the methods used to remove the effects of the atmosphere. The answer is only as good as the atmospheric correction.

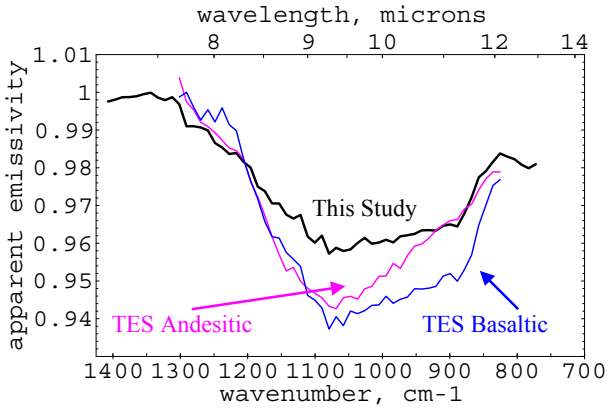

Figure 5: The top curve shows the same dark region plot as in figure 4. The middle and bottom curves are spectra kindly provided by Dr. J. Bandfield for the andesitic and basaltic (respectively) type regions described by the TES team in [7]. Note consistency in broad U-shape between the basaltic type region and the region of this study.

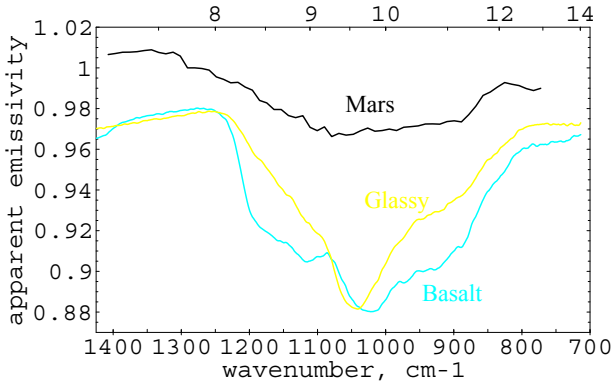

Figure 6: The top curve shows the same dark region plot as in figures 4 and 5. The middle curve plots a lab spectrum of glassy dark gray basalt, while the bottom curve plots a typical basalt spectrum [10,16]. Note the consistency in the overall broad envelope among the three plots.

References. [1] Schaber, G.G. (1982) *JGR*, 87, 9852-9866. [2] Christensen, P.R. (1982) *JGR*, 87, 9985-9998. [3] Christensen, P.R. (1986) *Icarus*, 68, 217-238. [4] Christensen, P.R., et al. (2000) *JGR*, 105, 9609-9621. [5] Mustard, J.F. and J.M. Sunshine (1995) *Science,* 267, 1623-1626. [6] Mustard, J.F., et al. (1997) *JGR,* 102, 25,605-25,615. [7] Bandfield, J.L., et al. (2000) *Science*, 287, 1626-1630. [8] Palluconi, F.D. and H.H. Kieffer. (1981) *Icarus*, 45, 415-426. [9] Edgett, K.S. and P.R. Christensen. (1991) *JGR*, 96, 22,765-22,776. [10] Salisbury, J.W., et al. (1991) *Infrared (2.1-25 micron) Spectra of Minerals,* JHU Press, Baltimore and London. [11] Schott, J.R. (1997) *Remote Sensing,* Oxford University Press, New York and Oxford. [12] Christensen, P.R. (2000) *JGR*, 105, 9507. [13] Christensen, P.R., et al. (1992) *JGR*, 97, 7719-7734. [14] Kirkland, L.E., P.B. Forney, and K.C. Herr (2000) *LPSC XXXI, abs. 1928*. [15] Johnson, B. R. (1998) *Aerospace Report ATR-99(8407)*. [16] ASTER web site, sample ba1b1f1s (the less V-shaped spectrum) of a dark gray basalt from Jordan; sample ba1b1fa (the V-shaped spectrum) of a dark gray basalt from Jordan. Both measured in hemispherical reflectance under the direction of J. Salisbury. [17] Christensen, P.R. and S.T. Harrison. (1993) *JGR,* 98(B11), 19,819-19,834. [18] Salisbury, J.W. and L.S. Walter. (1989) *JGR*, 94, 9192-9202. [19] Smith, M.D., et al. (2000) *JGR*, 105, 9589-9607. [20] Edget et al. (1994) *LPI Tech. Rpt., 94-04*, 25.